Assessment of the cabri transients power shape by using CFD and point kinetics codes

O. Clamens, J. Lecerf, B. Duc, J.-P. Hudelot, T. Cadiou, B. Biard

ASSESSMENT OF THE CABRI TRANSIENTS POWER SHAPE BY USING CFD AND POINT KINETICS CODES

Olivier Clamens, Johann Lecerf, Bertrand Duc, Jean-Pascal Hudelot
CEA, DEN, DER/SRES, Cadarache, F-13108 Saint Paul les Durance, France
jean-pascal.hudelot@cea.fr; olivier.clamens@cea.fr

Thierry Cadiou
CEA, DEN, DER/SESI, Cadarache, F-13108 Saint Paul les Durance, France

Bruno Biard
IRSN/PSN-RES/SEREX/L2EP, Cadarache, BP3 13115 Saint-Paul-Lez-Durance Cedex, France

ABSTRACT

This paper focuses on an approach to calculate the transient power shapes of the CABRI experimental pulse reactor. The ^{3}He depressurization of the CABRI transient rods are simulated using the STAR-CCM+ CFD[1] code. A good consistency is observed between computational and experimental results. The calculated gas depressurizations of the transient rods are then used to provide the transient power shapes by using the DULCINEE code based on point kinetics equations. The calculated transient power shapes results is lastly compared to experimental ones.

Key Words: **CABRI, CFD, kinetics, transient, depressurization**

1. INTRODUCTION

CABRI is an experimental pulse reactor operated by CEA[2] at the Cadarache research center. Since 1978 the experimental programs have aimed at studying the fuel behavior under Reactivity Initiated Accident (RIA) conditions. In order to study the PWR high burn up fuel behavior, the facility was modified to have a water loop able to provide thermal-hydraulic conditions representative of the nominal operating of PWR (155 bar, 300°C). This project which began in 2003 was driven within a broader scope including an overall facility refurbishment and a safety review. The global modification is conducted by CEA. The experiments take place in the framework of the OECD/NEA Project CIP[3] which is conducted by IRSN[4]. IRSN finances the refurbishment and the operation of the CABRI reactor that is currently put at disposal of the IRSN for investigations into the safety of fuel. The power transients

[1] Computational Fluid Dynamics
[2] Commissariat à l'Énergie Atomique et aux Énergies Alternatives
[3] CABRI International Program
[4] Institut de Radioprotection et de Sûreté Nucléaire: Institute for Radioprotection and Nuclear Safety

are generated by a dedicated so-called transient rods system allowing the very fast depressurization of ^{3}He tubes positioned inside the CABRI core.

This paper focuses on a computational approach to design and assess the transient power shapes of CABRI. This approach is based on the use of a CFD calculation of the depressurization sequence chained with a point kinetics calculation to obtain the power shape. The first part focuses on the principle of operation of the transient rods system. Then, the CFD approach is developed including validation of the calculation scheme and results brought by the simulations. The last section focuses on chained point kinetics calculations and preliminary results.

2. PRESENTATION OF THE CABRI TRANSIENT RODS SYSTEM

CABRI is a pool-type reactor [1], with a core made of 1487 stainless steel clad fuel rods with 6% ^{235}U enrichment. The reactor is able to reach a $23.7\ MW$ power level for a steady state. The reactivity is controlled via a system of 6 bundles of 23 hafnium control and safety rods.

The key feature of the CABRI reactor is its reactivity injection system [2]. This device allows the very fast depressurization into a discharge tank of the ^3He (strong neutron absorber) previously introduced inside 96 tubes (so called "transient rods") located among the CABRI fuel rods. As the reactor is initially running at a low power ($\sim 100\ kW$), the rapid absorber depressurization leads the tested fuel rod (positioned in the center of the reactor) to be submitted to an important burst of power which decreases just as fast due to the Doppler effect and other delayed reactivity feedbacks (see Figure 1). The total energy deposit in the tested rod is adjusted by dropping the control and safety rods after the power transient.

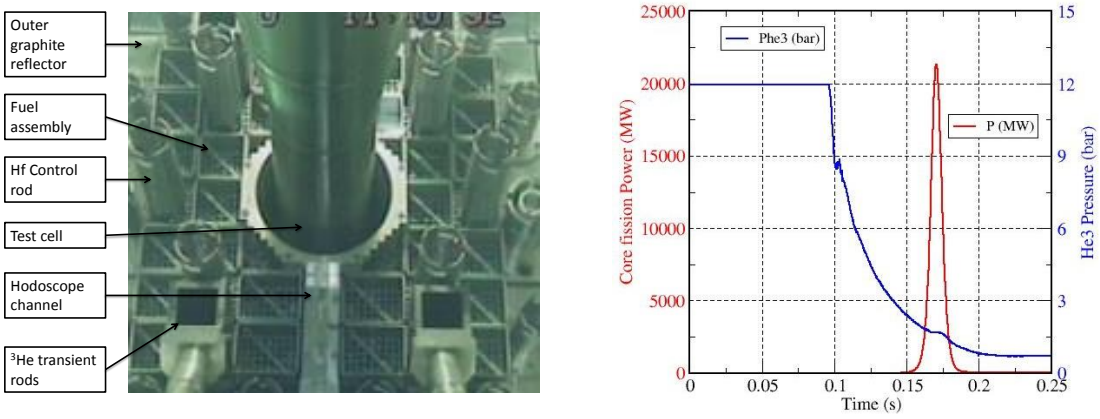

Figure 1. Radial cut of the CABRI core (left) - Typical CABRI ^{3}He Pressure and core power shapes during a RIA transient (right)

The CABRI transient rods system is made of the following main components (see Figure 2):

- 4 fuel assemblies (7x7 pins) equipped on their periphery with 24 tubes instead of 24 fuel rods. These tubes are connected together in the upper part of each assembly in order to join a line which leads to a principal collector.
- From the top of this collector two flow channels (low and high flow rates) lead to a $1000\ l$ discharge tank set under vacuum before operation. The low flow rate and high flow rate channels are equipped with a fast-opening valve (respectively small and large diameter) followed by a controlled valve.
- The 4 transient assemblies are pressurized to the target pressure ($14.85\ bar$ maximum) by the use of a compressor which pumps the ^{3}He from its storage tank via a devoted circuit.
- A specific control device triggers the different orders of the experimental sequence as for the aperture of the two fast-opening valves and the shutdown of the reactor control rods.
- For design and safety reasons, pressure cannot be measured directly in transient rods. Two different pressure transducers measure the ^{3}He pressure at the inlet of the collector. One goal of the simulation is to get the gas pressure in the transient rods knowing the pressure in the collector.

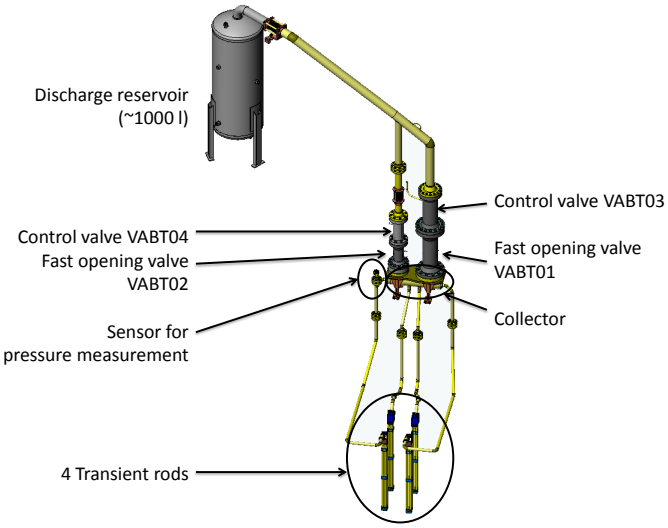

Figure 2. Main components of the CABRI transient rods

The transient rods depressurization causes the absorber ejection that induces a reactivity injection possibly reaching about 4$ in few milliseconds. The characteristics of the transient (maximum power, Full Width at Half Maximum (FWHM) and energy deposit) depend on the experimental sequence applied to the fast valves and on the adjustment of the associated controlled valves. Thus the short FWHM power transients, so called "natural transients", will be generated by the opening of the unique high flow rate channel. The maximum power is then very high (20 to 30 GW) and the FWHM is short ($\sim$ 10 ms) due to Doppler effect and other delayed reactivity feedbacks. The energy deposit in this

case depends on the initial pressure in the transient rods, the control valve aperture and the control rods drop time after transient

In order to be representative of other accidental power plant conditions, it is necessary to be able to increase the FWHM of the transient. This can be done by opening successively the fast opening valves of the low and then the high flow rate channels. The adjustment of the time difference between the apertures of the fast opening valves allows to generate so called "structured transients" characterized by FWHM varying from 20 to 80 ms. A good precision on this time difference is very important for the respect of the experimental goal. For those last transients, the final energy deposit in the tested fuel rod depends on the initial ^{3}He pressure but can also be adjusted by the control rods drop instant.

3. CFD APPROACH TO CALCULATE THE TRANSIENT RODS DEPRESSURIZATION

The CFD modeling, contrary to an analytical approach, can precisely handle complex geometry. The pressure evolution is calculated in the entire circuit, not only at the sensor location.

3.1. CFD calculation scheme and input data

A numerical simulation based on a CFD approach with the STAR-CCM+ software is selected. The STAR-CCM+[3] code allows any fluid flow in a complex geometry to be described. A CFD calculation is divided into three parts:

- Geometrical modeling of the fluid physical domain (boundary conditions, physical properties of ^{3}He), domain mesh;
- Solving Navier-Stokes equations using the CFD solver;
- Post-processing and analysis of results of temperature, pressure and speed.

The selected physical models are:

- 3D modeling;
- The RANS[5] approach to solve the Navier-Stokes equations;
- Using a turbulence model. The usual k-ϵ model consists in representing the effects of turbulence and eddy diffusivity by a turbulent viscosity. This eddy viscosity is calculated according to the

[5] Reynolds Averaged Navier-Stokes

turbulent energy k per mass unit, and energy dissipation ϵ per mass unit. Each of these two terms is the solution of a transport equation;

- Wall laws "All y + wall treatment" for approximating boundary layers;
- Unsteady calculation with the implicit solver.
- The ^{3}He is considered as an ideal gas. Laws of evolution of thermal conductivity [4] and dynamic viscosity [5] of ^{3}He vs. temperature were implemented in the simulation.

3.1.1. Meshing of the Transient Rods circuit

The first step of the simulation concerned the creation of the geometry of the transient rod system and its optimized meshing. The real geometry (see Figure 3) was obtained extracting the fluid part from computer-aid design geometry. This geometry was then cut in separate regions to which different types of meshing and/or physical or initial conditions were applied. A Trimmer-type meshing, with a mesh parameter of about $10\ mm$ was chosen. In order to well model wall treatment, 2 prism layers are meshed at the boundary layers. The overall geometry is composed of about 700000 cells. A special attention was paid to the meshing of the fast-opening valves moving during the firsts $3\ ms$ of simulation. To address this problem, the morphing method (see Figure 3) was used [3]. This adaptive meshing method consists in compacting or stretching meshes between two surfaces getting closer or going away from each other.

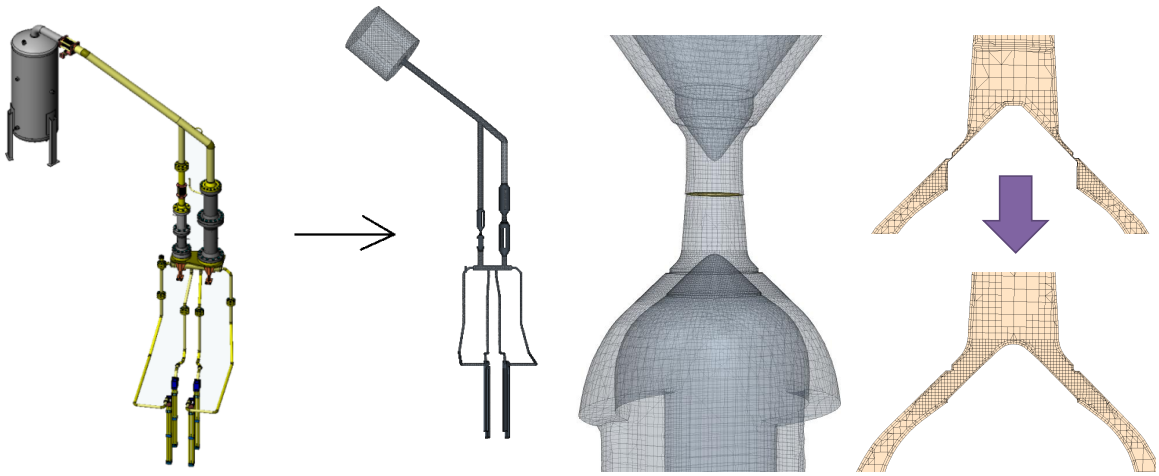

Figure 3. Fluid extraction (left) and fast valve VABT02 mesh morphing (right)

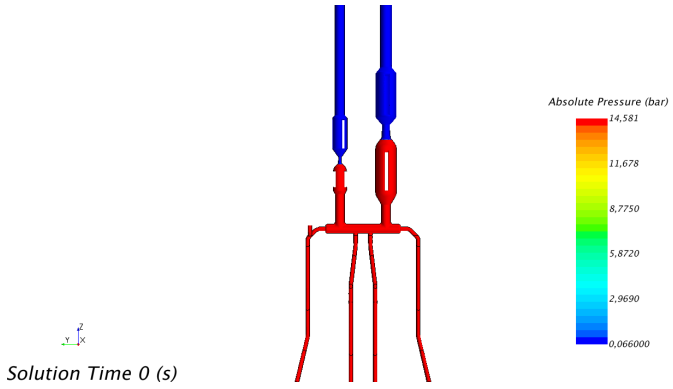

Figure 4. Pressure distribution before transient rods depressurization

3.1.2. Initial and boundary conditions

The circuit is divided in 2 areas: one high pressure area (varying from 1 to 14.85 bar before depressurization) in the upstream part of the flow and a low pressure area (fixed at 66 mbar). The pressure repartition is shown on the Figure 4. Heat exchanges between the outside environment ($\sim 293\ K$) and the transient rods circuit (from 100 to $800\ K$) are modeled. Heat transfer coefficients were calculated using thickness and properties of zircaloy[6] (rods) and stainless steel[7] (the rest of the circuit).

3.2. Validation of the CFD calculation scheme

A calculation scheme is validated when it possesses a satisfactory range of accuracy consistent with the intended application[8]. First, we will address the numerical validation of the meshing method and of the chosen physical models. Then, we will proceed to the experimental validation by comparing CFD results to past existing experimental depressurizations.

3.2.1. Numerical validation by comparing computational solutions to highly accurate solutions

The goal of the numerical validation step is to evaluate and minimize the numerical error linked to the mesh and the physical models. The first step of model numerical validation consists in showing that the chosen models are adapted to the studied case. The most important phenomenon here is the fast depressurization following the fast valve brutal opening. So the chosen models were tested on a simple geometry (see Figure 5) representative of the real geometry but analytically resolvable assuming an adiabatic flow. The solution of the problem is described in Appendix A leads to an equation (1) linking

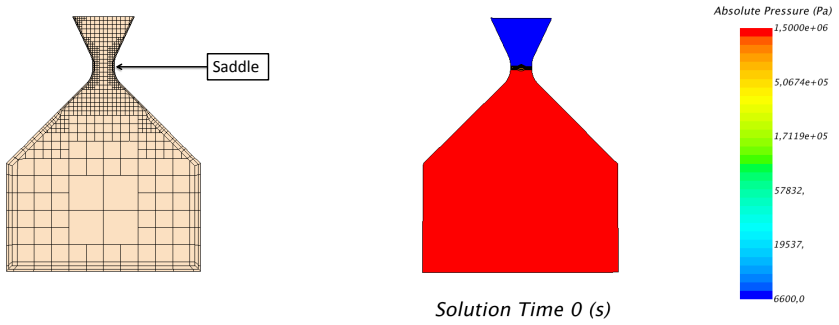

Figure 5. Simplified geometry mesh (left) and initial pressure conditions (right).

the averaged upstream pressure to the depressurization time.

$$P(t) = P_0(\frac{m(t)}{m_0})^{\gamma} = P_0[Bt+1]^{\frac{-2\gamma}{\gamma-1}} \tag{1}$$

The averaged pressure in the upstream part of the saddle was reported and monitored during the simulation. A typical example of simulation is the depressurization of a volume $V = 52\,l$ (actual volume of the transient rods) of Natural helium depressurization by a critical section of $2000\ mm^2$ (same order of magnitude as for the studied valves). The final curve was exported and compared to the analytical solution (see Figure 6). As we can see on Figure 6, curves are almost superimposed ($\Delta P(t) < 5\ \%$ in every case) on each other. The simulation was also realized for different gases (^3He, N_2) and different saddle sections. All lead to satisfactory results.

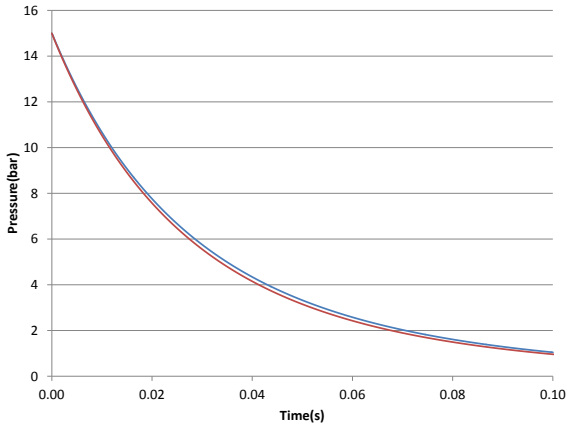

Figure 6. Comparison between analytical (red curve) and CFD (blue curve) solution of the depressurization

Another facet of the numerical validation process is to show that the CFD simulation precision is little affected by the mesh optimization. The same initial conditions were applied to different meshings of

the geometry. Figure 7 shows 2 depressurizations curves calculated at the location of the sensor (see Figure 2): one with the optimized mesh ($\sim 700,000$ cells) and the other for a finer mesh ($\sim 1,700,000$ cells).

All this demonstrates that the chosen physical models and meshing method are well suited for the studied case.

Note that a third curve was added to the Figure 7 to represent the evolution of the average pressure in the high pressure area (i.e. Figure 4). This third curve demonstrates that the measure location has an influence on the depressurization curve shape. However, CFD simulations show that after a certain time (function of the depressurization speed), pressures tend toward the same value in all the high pressure area.

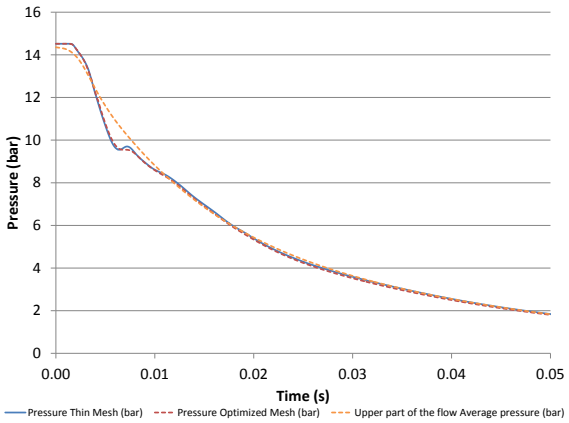

Figure 7. CFD sensor depressurization for the thin and the optimized mesh

3.2.2. Experimental Validation by comparing CFD results with experimental depressurizations

Before extracting depressurizations curves in the transient rods from the simulations, we need to be sure that simulation represents well reality. Hence, the simulation is validated by comparison with experimental data. The valves apertures were adjusted to represent reality as well as possible. The results of this study are presented on Figure 8 with two representative cases. In addition to give the good global shape fo depressurization curves, measured pressure fluctuations are also calculated and well reproduced by CFD simulation. A very good consistency is observed between the computational and experimental results obtained at the sensor level. Hence, we can also assume that the calculated depressurization in the transient rods is also close to reality.

Figure 8 also introduces the calculation of depressurization inside the transient rods. The depressurization begins later ($\sim$5 ms after the simulation start) in the transient rods because the rods are located at $\sim$ 4 m from the valves.

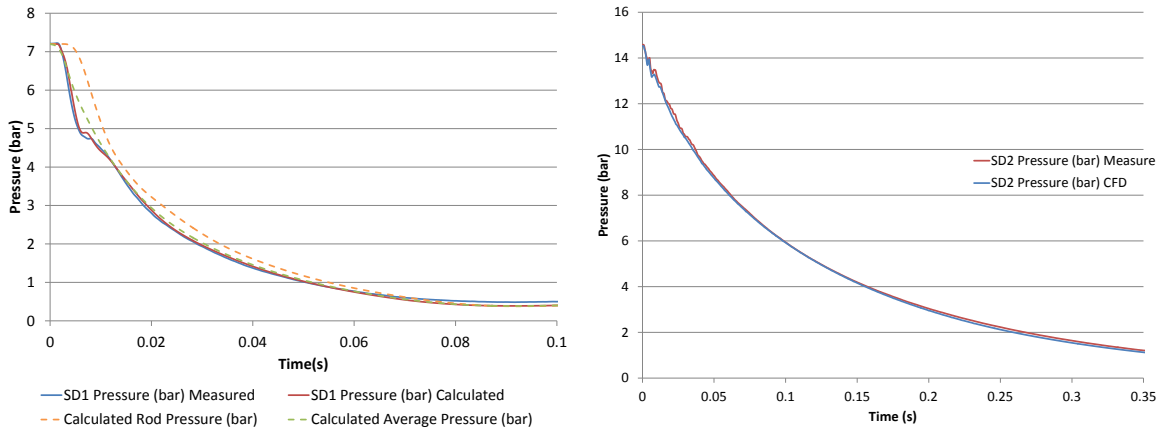

Figure 8. Comparison between measured and calculated depressurizations. SD1: Simple Depressurization by high flow rate channel (left) - SD2: Simple Depressurization by low flow rate channel (right)

4. ASSESSMENT OF POWER TRANSIENTS USING THE DULCINEE CODE

These calculated gas depressurizations of the transient rods can be used to design or predict the transient power shape by using the DULCINEE code based on point kinetics equations. This code has been successfully tested against experimental data acquired during CABRI past programs (several hundred power bursts in the past 40 years) [9].

DULCINEE was developed in the 1970s [10] to design and characterize the behavior of a nuclear core with low pressure coolant (water, sodium, etc.) during several types of transients (RIA, LOF, ramps, overpower, LOCA). DULCINEE embeds simplified thermal and thermal hydraulics models. The thermal hydraulics can process single or double phase flows in forced convection. Pressure and flow rate are computed according to the local void fraction with dedicated correlations. Heat transfer in the fuel rods is modeled from the inside to the outside. Several types of regions are described (fuel/gap/clad). The physical properties of each region are tabulated as a function of the temperature. The CABRI core is modeled with 2 regions: 1 hot channel and the remaining average channels.

DULCINEE allows assessing the transient power shape from the knowledge of the external reactivity as a function of time. This last one can be evaluated with a combination of functions as follows:

$$\rho(t) = \rho(P_{^3He}) \otimes P_{^3He}(t) \tag{2}$$

$\rho(P_{^3He})$ is given by real geometry neutronic calculations [11, 12] using the French stochastic TRIPOLI-4 code [13] and the JEFF 3.1.1 nuclear data library [14], $P_{^3He}(t)$ corresponds to ^3He pressure evolution in the transient rods, for instance determined by CFD calculations as presented in sections 3.1 and 3.2. As input data, DULCINEE also uses neutronic parameters that were computed with TRIPOLI 4 (using the JEFF3.1.1 nuclear database): Doppler coefficient, effective fraction of delayed neutrons and neutron generation lifetime. It also takes into account other delayed phenomena like clad expansion or coolant

density. After every temperature step, the neutron feedbacks can be re-assessed in order to provide the overall system net reactivity as an input of the point kinetics equations computed in DULCINEE. Hence the time step is incremented and an ulterior situation is computed, applying the point kinetics equation to a sequence of stationary thermal conditions. An example of assessment of a transient power shape using DULCINEE is given in Figure 9.

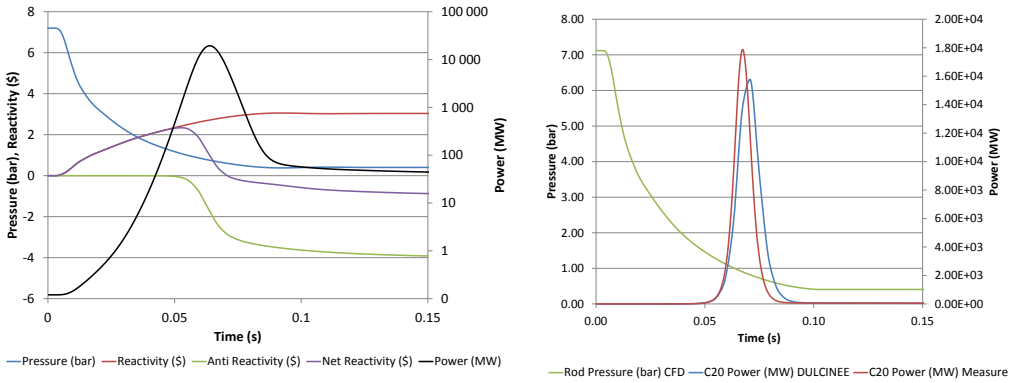

Figure 9. Computation with DULCINEE of a power transient using calculated gas pressure in transient rods. Case of a single depressurization from 7.2 bar (gas purity: 99.5%) though the high flow rate channel with the control valve fully opened (left)- Comparison of a computed power shape with measure for the C20 experiment (right)

The comparison presented in Figure 9 is based on a measure done in the 90's when CABRI was still in sodium experimental loop configuration. The power transient of the C20 test was produced by the simple depressurization of the high flow rate channel (control valve fully opened) with Helium 3 (96% pure) pressurized to 7.2 bar. The maximum power (16 GW) of the calculated transient is lower than the experimental one (18 GW), but the FWHM is higher (11 ms vs 9 ms). The computed energy deposit in the core (210 MJ) is higher than the measured one (188 MJ). More generally, it is always observed that DULCINEE over predicts the energy deposit in the core.

5. CONCLUSION

The ^{3}He depressurizations of the CABRI transient rods were calculated using the STAR-CCM+ CFD code. After the numerical validation, the initial conditions and the physical properties, a very good consistency is observed on depressurization curves between computational and experimental results. These calculated gas depressurizations of the transient rods are then used to provide the transient power shape by using the DULCINEE code based on point kinetics equations. In every case, power shapes during transients are rather well reproduced by simulation, but with a slight over-prediction of the energy deposit and of FWHM. Further investigations will be performed in the mean future to identify if a 3D kinetics approach would allow reducing those deviations and thus improving the accuracy of the transient shape prediction.

ACKNOWLEDGMENTS

The authors would like to thank the French Institute of Safety and Radiation Protection (IRSN) contributing to the study financing.

REFERENCES

[1] "CABRI." In: *PHYSOR* (2016).

[2] Bertrand Duc *et al.* "Renovation, improvement and experimental validation of the helium-3 transient rods system for the reactivity injection in the cabri reactor." In: *International Group On Research Reactors*. Bariloche, Argentina, November 17 - 21 (2014).

[3] CD-Adapco User Guide. "Star-ccm+ version (10.02)." (2015).

[4] B. Le Neindre. *Conductivite thermique des liquides et des gaz.* Techniques Ingenieur (1996).

[5] —. *Viscosite gaz pression atmospherique*. Ed. Techniques Ingenieur (2005).

[6] Y. Kim, J. Park, and J. Cleveland. "Thermophysical properties database of materials for light water reactors and heavy water reactors." *IAEA, Vienna* (2006).

[7] M. Laurent and P.-L. Vuillermoz. "Conductivite thermique des solides." *Techniques de l'ingenieur. Constantes physico-chimiques*, **3(K420)**: pp. K420–1 (1993).

[8] W. L. Oberkampf and T. G. Trucano. "Verification and validation in computational fluid dynamics." *Progress in Aerospace Sciences*, **38(3)**: pp. 209–272 (2002).

[9] Guillaume Ritter, Remi Berre, and Laurent Pantera. "DULCINEE. beyond neutron kinetics, a powerful analysis software." In: *RRFM IGORR*. Prague, Czech Republic, March 18 - 22 (2012).

[10] P. Dutraive, S. Fabrega, and F. Millot. "DULCINEE code (DULCINEE code for water cooled reactor at low pressure)." (1970).

[11] O. Gueton *et al.* "Neutronics computations in support of the CABRI core safety analysis." In: *IGORR*. Benjin, China, October 28 - 30 (2009).

[12] J.-P. Hudelot *et al.* "Development, validation and qualification of neutronics calculation tools for small reactors - application to the JHR, CABRI and OSIRIS reactors." In: *RRFM 2012 Conference*. Prague, Czech Republic, March 18 - 22 (2012).

[13] E. Brun *et al.* "Overview of TRIPOLI-4 version 7, continuous-energy monte carlo transport code." (2011).

[14] A. Santamarina *et al.* "The JEFF-3.1. 1 nuclear data library." *JEFF report*, **22(10.2)**: p. 2 (2009).

APPENDIX A. SIMPLE DEPRESSURIZATION ANALYTICAL SOLUTION

$$\frac{\rho_0}{\rho^*} = (\frac{\gamma+1}{2})^{\frac{1}{\gamma-1}}, \quad \frac{T_0}{T^*} = (\frac{\gamma+1}{2}), \quad \frac{P_0}{P^*} = (\frac{\gamma+1}{2})^{\frac{\gamma}{\gamma-1}} \tag{3}$$

Those are the relations for a sonic flow with ρ_0: stopping gas density, ρ^*: critical gas density, $\gamma = \frac{Cp}{Cv}$: Laplace coefficient, T_0: stopping gas temperature, T^*: critical gas temperature, P_0: stopping gas pressure, P^*: critical gas pressure.

$$c^* = \sqrt{\gamma r T^*} \quad c^*\text{: saddle speed of sound, } r = \frac{R}{M}\text{: specific gas constant} \tag{4}$$

$$\text{Isentropic Laplace law for ideal gases:} \quad PV^\gamma = cst \tag{5}$$

Mass flow is related to the saddle section A^* by the following equation:

$$Q_m = -\dot{m} = \rho^* A^* c^* \quad <=> \quad -\dot{m} = \rho(\frac{\gamma+1}{2})^{\frac{1}{1-\gamma}} A^* \sqrt{\gamma r T^*} \tag{6}$$

$$<=> \quad -\dot{m} = \frac{m}{V}(\frac{\gamma+1}{2})^{\frac{1}{1-\gamma}} A^* \sqrt{\gamma r T (\frac{2}{\gamma+1})} = \frac{m}{V}(\frac{\gamma+1}{2})^{\frac{1}{1-\gamma}} A^* \sqrt{\gamma r (\frac{PV}{mr})(\frac{2}{\gamma+1})} \tag{7}$$

Using (5), we deduce an expression for P:

$$P_0 V^\gamma = P V_{tot}^\gamma => \quad -\dot{m} = \frac{m}{V}(\frac{\gamma+1}{2})^{\frac{1}{1-\gamma}} A^* \sqrt{\gamma r (\frac{P_0 (\frac{V}{V_{tot}})^\gamma V}{mr})(\frac{2}{\gamma+1})} \tag{8}$$

Where the definition of V_{tot} is set by the mass conservation:

$$\rho V_{tot} = \rho_0 V \quad => \quad -\dot{m} = \frac{m}{V}(\frac{\gamma+1}{2})^{\frac{1}{1-\gamma}} A^* \sqrt{\gamma r \frac{T_0}{\frac{m}{m_0}} (\frac{\rho}{\rho_0})^\gamma (\frac{2}{\gamma+1})} \tag{9}$$

$$<=> \quad -\dot{m} = \frac{m}{V}(\frac{\gamma+1}{2})^{\frac{1}{1-\gamma}} A^* \sqrt{\gamma r \frac{T_0}{\frac{m}{m_0}} (\frac{m}{m_0})^\gamma (\frac{2}{\gamma+1})} \tag{10}$$

We recognise the initial critical speed c_0^* and define the critical time t_c^* to simplify the equation:

$$c_0^* = \sqrt{\gamma r T_0 (\frac{2}{\gamma+1})}\,, \; t_c^* = \frac{V}{A^* c_0^*} \quad => \quad -\dot{m} = \frac{m}{t_c^*}(\frac{\gamma+1}{2})^{\frac{1}{1-\gamma}} (\frac{m}{m_0})^{\frac{\gamma-1}{2}} \tag{11}$$

By integration, the differential equation solution is:

$$m = m_0 [Bt+1]^{\frac{-2}{\gamma-1}} \quad => \quad -\dot{m} = \frac{2B}{\gamma-1} m (\frac{m}{m_0})^{\frac{\gamma-1}{2}} \tag{12}$$

$$\frac{1}{t_c^*}(\frac{\gamma+1}{2})^{\frac{1}{1-\gamma}} = \frac{2B}{\gamma-1} \quad => \quad \frac{\gamma-1}{2t_c^*}(\frac{\gamma+1}{2})^{\frac{1}{1-\gamma}} = B \tag{13}$$

$$=> \quad P(t) = P_0 (\frac{m(t)}{m_0})^\gamma = P_0 [Bt+1]^{\frac{-2\gamma}{\gamma-1}} \tag{14}$$